AFRL-RX-WP-JA-2015-0116

FATIGUE AND FRACTURE BEHAVIOR OF A Ca-BASED BULK-METALLIC GLASS (POSTPRINT)

O.N. Senkov and D.B. Miracle
AFRL/RXCM

J. Raphael
Columbus McKinnon Corporation

G.Y. Wang and P.K. Liaw
The University of Tennessee

APRIL 2014
Interim Report

AIR FORCE RESEARCH LABORATORY
MATERIALS AND MANUFACTURING DIRECTORATE
WRIGHT-PATTERSON AIR FORCE BASE OH 45433-7750
AIR FORCE MATERIEL COMMAND
UNITED STATES AIR FORCE

NOTICE AND SIGNATURE PAGE

Using Government drawings, specifications, or other data included in this document for any purpose other than Government procurement does not in any way obligate the U.S. Government. The fact that the Government formulated or supplied the drawings, specifications, or other data does not license the holder or any other person or corporation; or convey any rights or permission to manufacture, use, or sell any patented invention that may relate to them.

Qualified requestors may obtain copies of this report from the Defense Technical Information Center (DTIC) (http://www.dtic.mil).

AFRL-RX-WP-JA-2015-0116 HAS BEEN REVIEWED AND IS APPROVED FOR PUBLICATION IN ACCORDANCE WITH ASSIGNED DISTRIBUTION STATEMENT.

//Signature//

MICHEAL E. BURBA, Project Engineer
Metals Branch
Structural Materials Division

//Signature//

DANIEL J. EVANS, Chief
Metals Branch
Structural Materials Division

//Signature//

ROBERT T. MARSHALL, Deputy Chief
Structural Materials Division
Materials And Manufacturing Directorate

This report is published in the interest of scientific and technical information exchange and its publication does not constitute the Government's approval or disapproval of its ideas or findings.

REPORT DOCUMENTATION PAGE

Form Approved
OMB No. 0704-0188

1. REPORT DATE *(DD-MM-YY)*	2. REPORT TYPE	3. DATES COVERED *(From - To)*
April 2014	Interim	19 March 2014 – 31 March 2014

4. TITLE AND SUBTITLE
FATIGUE AND FRACTURE BEHAVIOR OF A Ca-BASED BULK-METALLIC GLASS (POSTPRINT)

5a. CONTRACT NUMBER
In-house

5b. GRANT NUMBER

5c. PROGRAM ELEMENT NUMBER
62102F

6. AUTHOR(S)
See back

5d. PROJECT NUMBER
4349

5e. TASK NUMBER

5f. WORK UNIT NUMBER
X0W6

7. PERFORMING ORGANIZATION NAME(S) AND ADDRESS(ES)
See back

8. PERFORMING ORGANIZATION REPORT NUMBER

9. SPONSORING/MONITORING AGENCY NAME(S) AND ADDRESS(ES)
Air Force Research Laboratory
Materials and Manufacturing Directorate
Wright-Patterson Air Force Base, OH 45433-7750
Air Force Materiel Command
United States Air Force

10. SPONSORING/MONITORING AGENCY ACRONYM(S)
AFRL/RXCM

11. SPONSORING/MONITORING AGENCY REPORT NUMBER(S)
AFRL-RX-WP-JA-2015-0116

12. DISTRIBUTION/AVAILABILITY STATEMENT
Distribution Statement A. Approved for public release; distribution unlimited.

13. SUPPLEMENTARY NOTES
Journal article published in *Metallurgical and Materials Transactions A*, Volume 41A, July 2010, 1775-1779. This report contains color. The final publication is available at DOI: 10.1007/s11661-009-0024-x.

14. ABSTRACT

The compression and fatigue behavior of a $Ca_{65}Mg_{15}Zn_{20}$ bulk-metallic glass (BMG) was studied in air at room temperature. During the preparation of cubical samples of the $Ca_{65}Mg_{15}Zn_{20}$ for compression and fatigue investigations, small spherical cavities were found. Under both monotonic and cyclic compression loadings of the samples, fractures initiated at these cavities and propagated in a direction generally parallel to the loading axis. Finite-element analysis (FEA) was used to model the fracture behavior. The FEA of a centrally located spherical void showed that under compression loading, large tensile stresses evolved in the cavities. The orientation of the maximum principal stress (P1) was found to be normal to the direction of crack propagation, which is consistent with the experimental finding. Stresses in deeply embedded adjacent voids and those in superficial voids were also studied. The influence of the void location in the cubical sample on the fracture behavior was quantitatively discussed.

15. SUBJECT TERMS
fatigue, fracture, compression testing, bulk metallic glasses

16. SECURITY CLASSIFICATION OF:			17. LIMITATION OF ABSTRACT:	18. NUMBER OF PAGES	19a. NAME OF RESPONSIBLE PERSON (Monitor)
a. REPORT	b. ABSTRACT	c. THIS PAGE			Micheal E. Burba
Unclassified	Unclassified	Unclassified	SAR	9	19b. TELEPHONE NUMBER *(Include Area Code)* (937) 255-9795

REPORT DOCUMENTATION PAGE Cont'd

6. AUTHOR(S)

O.N. Senkov and D.B. Miracle - AFRL/RXCM

J. Raphael - Columbus McKinnon Corporation

G.Y. Wang and P.K. Liaw - The University of Tennessee

7. PERFORMING ORGANIZATION NAME(S) AND ADDRESS(ES)

AFRL/RXCM
2941 Hobson Way
Bldg 654, Rm 136
Wright-Patterson AFB, OH 45433

Research and Development Group
Columbus McKinnon Corporation
Damascus, VA 24236

Department of Material Science and Engineering
The University of Tennessee
Knoxville, TN 37996

Fatigue and Fracture Behavior of a Ca-Based Bulk-Metallic Glass

J. RAPHAEL, G.Y. WANG, P.K. LIAW, O.N. SENKOV, and D.B. MIRACLE

The compression and fatigue behavior of a $Ca_{65}Mg_{15}Zn_{20}$ bulk-metallic glass (BMG) was studied in air at room temperature. During the preparation of cubical samples of the $Ca_{65}Mg_{15}Zn_{20}$ for compression and fatigue investigations, small spherical cavities were found. Under both monotonic and cyclic compression loadings of the samples, fractures initiated at these cavities and propagated in a direction generally parallel to the loading axis. Finite-element analysis (FEA) was used to model the fracture behavior. The FEA of a centrally located spherical void showed that under compression loading, large tensile stresses evolved in the cavities. The orientation of the maximum principal stress (P1) was found to be normal to the direction of crack propagation, which is consistent with the experimental finding. Stresses in deeply embedded adjacent voids and those in superficial voids were also studied. The influence of the void location in the cubical sample on the fracture behavior was quantitatively discussed.

DOI: 10.1007/s11661-009-0024-x

I. INTRODUCTION AND OUTLINE OF THE PROBLEM

BULK-METALLIC glasses (BMGs) lack grain boundaries and any long-range order. Therefore, they are significantly different from crystalline materials. The BMGs have many excellent physical and chemical properties, such as high strengths, high elastic limits, high wear and corrosion resistances, almost perfect as-cast surfaces, and good fracture toughness.[1,2] Since BMGs can be applied as potential structural materials, the mechanical behavior of BMGs is being studied extensively.[3–8]

The Ca-based BMGs have many unique properties, such as low density (~2.0 g/cc), low Young's modulus (~20 to 30 GPa), low shear modulus (~8 to 15 GPa), low glass-transition temperature (T_g ~ 100 °C to 190 °C), and low crystallization temperature (T_x ~ 130 °C to 240 °C).[8–11] Moreover, Ca-based BMGs have very good glass-forming ability (GFA). The elastic modulus of Ca-based BMGs is comparable to that of human bones, and Ca, Mg, and Zn are biocompatible.[11] These features make the Ca-Mg-Zn–based alloys attractive for use in biomedical applications.[10] Since Ca-based BMGs were successfully synthesized,[12,13] Ca-based BMGs are attracting more and more attention.

In a previous article,[14] the monotonic compression and compression-compression fatigue experiments were employed to investigate the mechanical properties of the $Ca_{65}Mg_{15}Zn_{20}$ (at. pct) BMG at room temperature in air. Cubical samples, 4 mm on a side, were prepared. Under compression loading, it was observed that fractures originated from small deeply embedded spherical voids, typically 25 to 50 μm in diameter, which functioned as crack-nucleation sites. The alloy was macroscopically brittle and crack propagation occurred in a direction nearly parallel to the loading axis, which demonstrated a dominant splitting failure with fracture planes from 0 to 20 deg relative to the loading axis. Figure 1 demonstrated an example of splitting fracture under monotonic-compression loading. In general, this splitting fracture is observed in brittle materials, including Fe-based BMGs.[14] This phenomenon could be caused by the brittleness of materials and voids in the materials. To explain the observed splitting behavior, finite-element analysis (FEA) was conducted in the current work.

II. FINITE-ELEMENT MODELING

In the finite-element method,[15] a structure is subdivided into a number of finite-sized volumes, called elements. In each element, the displacements, strains, and stresses are approximated by polynomial shape functions. Connections between elements are made through a finite number of grid points, commonly called nodes. Interactions among elements occur solely through the forces exerted at the grid points. Element material properties and a structure's geometry are used to develop the structure's stiffness characteristics. Known loads are applied at nodes to the structure

J. RAPHAEL, Engineer, is with the Research and Development Group, Columbus McKinnon Corporation, Damascus, VA 24236. G.Y. WANG, Research Assistant, and P.K. LIAW, Professor, are with the Department of Material Science and Engineering, The University of Tennessee, Knoxville, TN 37996. Contact e mail: gwang@utk.edu O.N. SENKOV and D.B. MIRACLE, Senior Scientists, are with the Air Force Research Laboratory, Materials and Manufacturing Directorate, Wright Patterson Air Force Base, Dayton, OH 45433.

This article is based on a presentation given in the symposium "Bulk Metallic Glasses VI," which occurred during the TMS Annual Meeting, February 15 19, 2009, in San Francisco, CA, under the auspices of TMS, the TMS Structural Materials Division, TMS/ASM: Mechanical Behavior of Materials Committee.

Article published online November 7, 2009

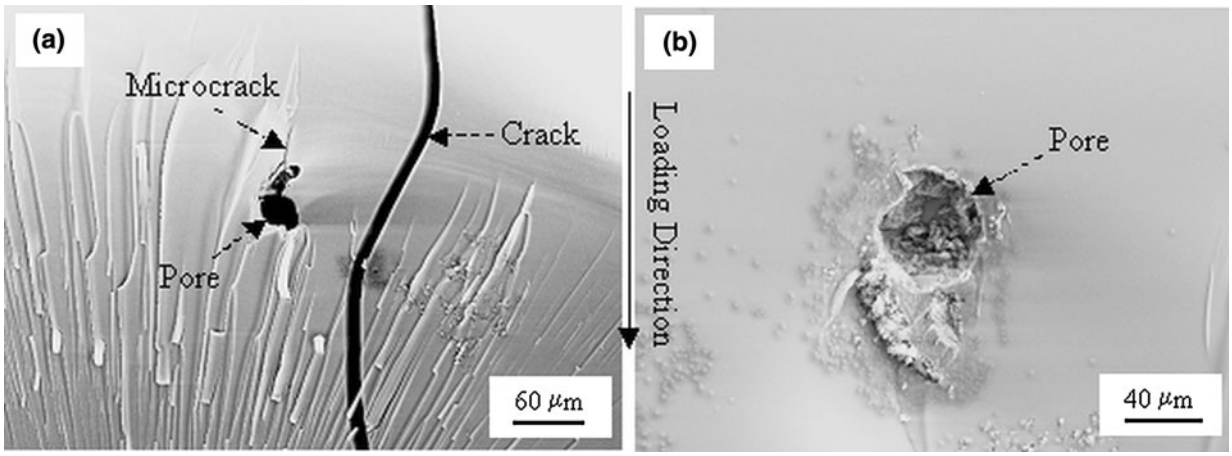

Fig. 1 SEM fractographs demonstrating (*a*) a porelike flaw, microcrack, and crack on the fracture surface; and (*b*) a porelike flaw, which resulted in macroscopic splitting failure under compression.[14]

with a given stiffness and the strain and stress distributions in the structure are calculated. The development of the finite-element model was straightforward. The necessary elements are the geometry, material properties, boundary conditions, loading, and element formulation.

The first case studied was that of a deeply embedded (2 mm from each face) centrally located void of 50-μm diameter, which shows both the solid model and the finite-element model. Results of this analysis demonstrate the essential nature of the stress distribution in the void. In addition, different failure theories could be applied to determine which would best explain the observed behavior of dominant splitting fracture. It was anticipated that the results of this analysis would, in addition to determining general stress levels, provide some insight into the void behavior, relative to the size and shape of the cubical sample.

Case 2 was the analysis of three inline 50-μm-diameter voids, with a center-to-center spacing of 150 μm. The results of this analysis allowed the effect of one void upon another to be assessed. It would show whether the stress concentration at one void had a meaningful effect upon the stress state in a nearby adjacent void.

Case 3 examined the stress distribution in a hemispherically shaped surface void. Although no fractures emanating from these voids were observed, it was nevertheless deemed important to learn if the stress distribution in superficial voids was fundamentally different from that of a deeply embedded void or if surface voids posed different risks.

The fourth and last case permitted an examination of the size effect. It was identical to case 1 with the exception that the void diameter was 100 μm, rather than 50 μm. If the stress state in a 100-μm-diameter void was to be more severe than that in a 50-μm-diameter void, then compression-compression fatigue performance could be improved by controlling the void size.

The FEA model used in case 1 was a cube, 2 mm on a side, with one octant of the centrally located void remaining. Since there are three planes of the geometrical and loading symmetry, it was only necessary to model one octant.

The $Ca_{65}Mg_{15}Zn_{20}$ is quite brittle and exhibits a purely linear stress/strain response up to the loading strains of ~1.5 pct. It has a Young's modulus of 20 GPa,[14] fracture strength of 364 MPa,[14] and Poisson's ratio of 0.30.[16]

Applied boundary conditions were zero normal displacements at all nodes on each plane of the symmetry. Model loading in all cases was a compressive displacement of 0.0254 mm applied in the x direction. This arrangement is equivalent to compressive strain of 1.27 pct.

In the case 2 finite-element model, due to the symmetry in both the geometry and loading, only one octant is required for the solution, since no displacements normal to the surfaces that define the symmetry can occur. Thus, only one-and-one-half voids are modeled.

Isoparametric brick elements with quadratic-shape functions were used throughout. NEi Nastran,[15] a displacement-based general purpose finite-element code, well suited to problems of this type, was used for the solution.

III. RESULTS

A partially-zoomed view of the case 1 maximum principal stress distribution is shown in Figure 2. The stress peak value is 180.28 MPa. Its location is indicated as point A in Figure 10. Point B, which is located on the surface of the void along the z-axis and has a zero stress level, is also noted in Figure 2. The maximum principal stress (P1) distribution along arc A-B is shown in Figure 3. In Figure 4, the same stress distribution is presented, but the viewing direction is parallel to the loading plane. The singular feature seen in Figure 4 is the circularity of the stress distribution. It is axisymmetric with respect to the x-axis. The deformed shape of the void is generally ellipsoidal, in which the

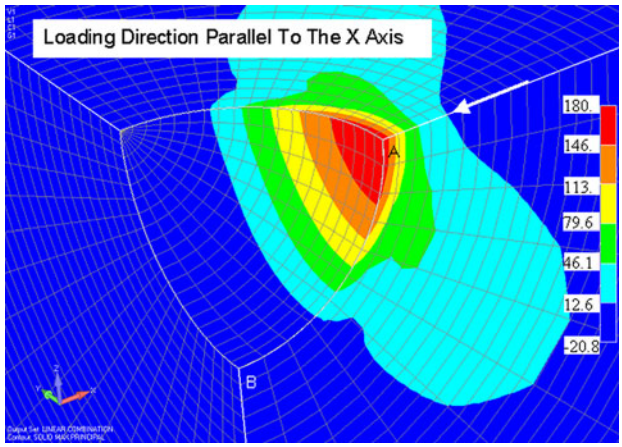

Fig. 2 Zoomed view of the maximum principal stress distribution in a deeply embedded 50 μm diameter spherical void (case 1). Arc A B has been identified. Units are MPa.

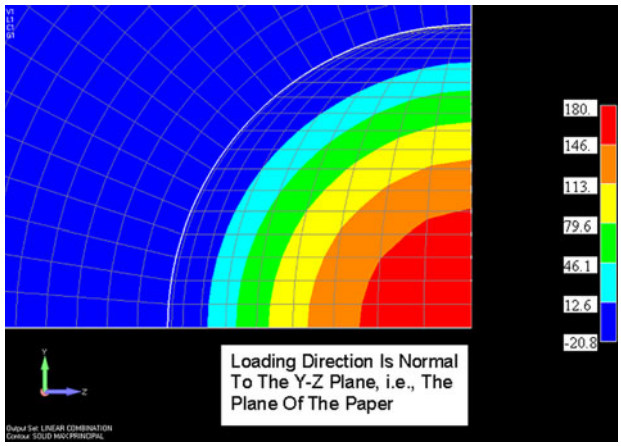

Fig. 4 Maximum principal stress distribution in a deeply embedded 50 μm diameter spherical void (case 1). The viewing direction is parallel to the applied load. Units are MPa.

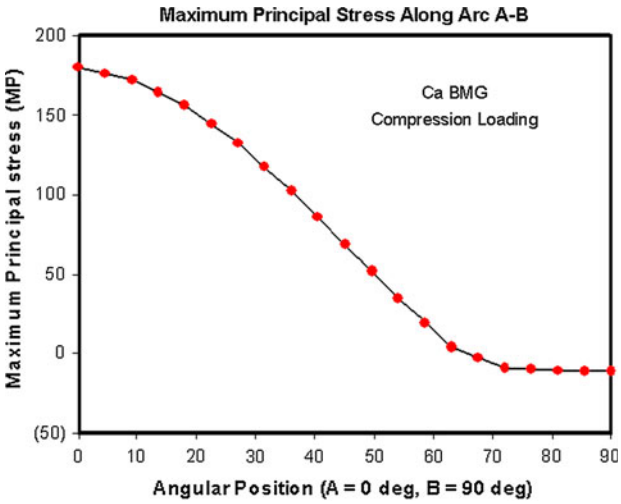

Fig. 3 Graph of the maximum principal stress distribution along arc A B in a deeply embedded 50 μm diameter spherical void (case 1). Figure 2 provides a definition of arc A B.

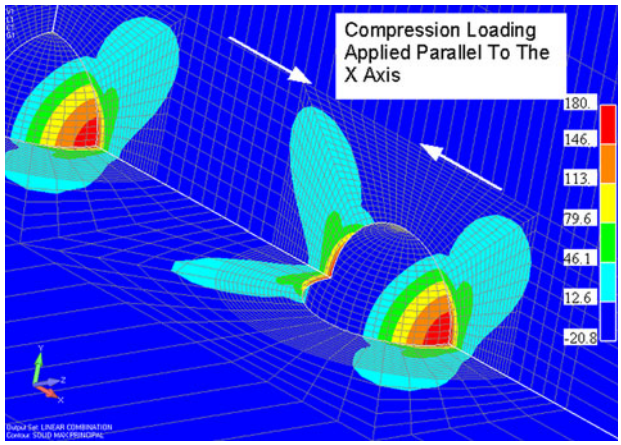

Fig. 5 Zoomed view of the maximum principal stress distribution in case 2. Note a similarity to case 1 results. Also note that the void shapes are different because there are three planes of symmetry in the centrally located void, but only two planes of symmetry in the void whose center is at an x coordinate of 150 μm. Units are MPa.

deformation is superimposed over the original geometry, which is shown in bold lines.

Case 2 results are shown in Figures 5 and 6. Figure 5 is a zoomed view of the maximum principal stress distribution in the vicinity of two adjacent voids. Figure 6 is a plot of the maximum principal-stress distribution along arc A-B-C. The maximum P1 values were observed to be 176.11 MPa, which is the same as case 1. Only small void-to-void differences (6.93 MPa) were found.

Case 3 results are seen in Figure 7. The maximum P1 value was 160.69 MPa, which is smaller than the value observed in case 1. In surface voids, the maximum principal stress distribution is not axisymmetric, but shows two pronounced stress concentrations. A graph of the maximum principal stress distribution passing through the two stress concentrations is presented in Figure 8.

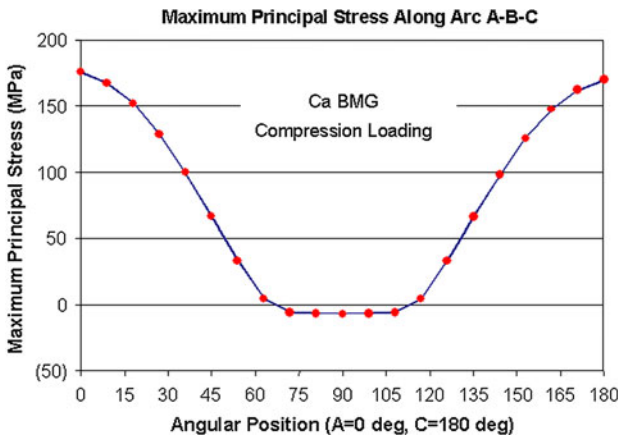

Fig. 6 Maximum principal stress distribution along arc A B C (case 2).

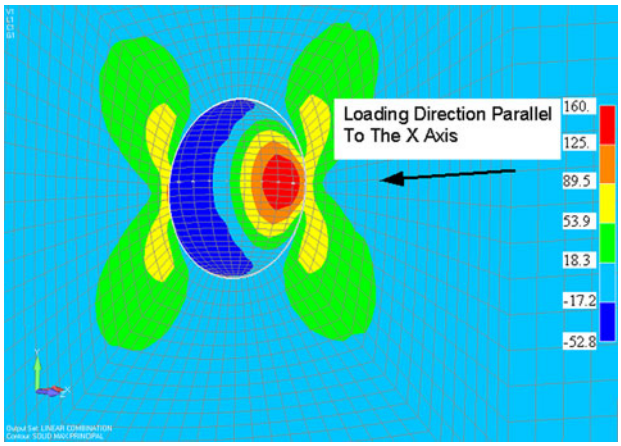

Fig. 7 Zoomed view of the maximum principal stress distribution for case 3. Note that the stress distribution does not manifest the kind of symmetry seen in other cases and that the peak value is less than that seen in other cases. Units are MPa.

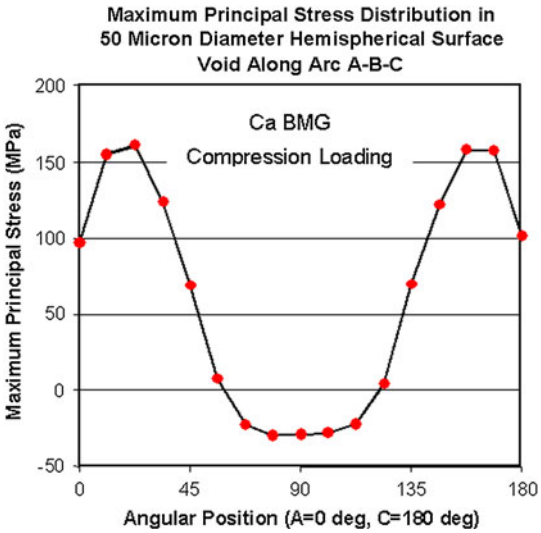

Fig. 8 Graph of the maximum principal stress distribution along arc A B C (case 3). Note the symmetry in the distribution and the fact that peak value is less than that in other cases.

Case 4 results are identical to those of case 1. Figure 9 is a graph that compares the P1 stress distribution in a 50-μm-diameter void to that in a 100-μm-diameter void. Since the FEA mesh in both cases contains the same number of elements in the void, the results reflect P1 values at corresponding angular locations along arc A-B, which is defined in Figure 2. There are essentially identical results for the 50- and 100-μm voids in Figure 9.

IV. DISCUSSION

From the case 1 results (Figures 2 through 4), we learn that the P1 distribution is axisymmetric. Since the specimen is a cube, we can conclude that the P1 distribution is unaffected by the general part shape.

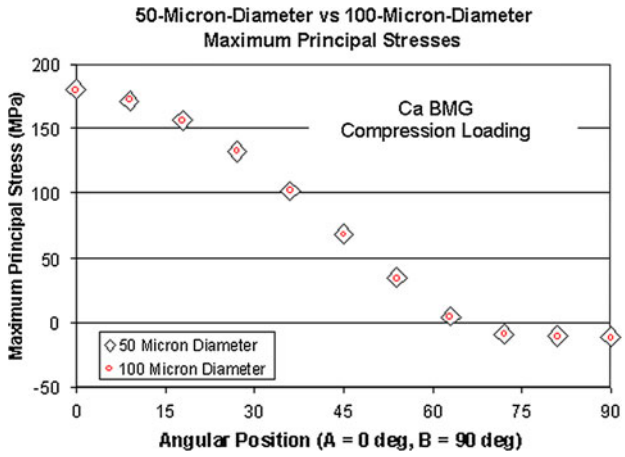

Fig. 9 Comparison of the maximum principal stress distributions in cases 1 and 4 along arc A B, which is defined in Fig. 2. Note that the values are very nearly identical at every nodal point. This fact confirms the conclusion that for small voids, P1 values are indepen dent of the void diameter.

This trend is not surprising, given that the overall dimensions of the part are so much larger than the void. Thus, the void behaves as though it were situated in a semi-infinite medium. The deformed geometry is generally ellipsoidal, with equal positive displacements occurring along the y- and z-axes, and a negative displacement along the z-axis. This change in the shape leads to a flattening of the void in the vicinity of the loading axis, resulting in localized stretching that causes large transverse tensile stresses. It is this tensile stress that is responsible for the observed splitting behavior.

Since the material's purely linear stress-strain response suggests a brittle failure mechanism, it is natural to apply the Rankine, or the maximum normal stress theory of failure.[17,18] Indeed, fractures do initiate at or very close to the point of the maximum principal stress, as predicted by the model. Any differences between the observed behavior and that predicted by the model are likely attributable to small deviations from the sphericity in actual voids. Crack propagation occurs in a direction parallel to the loading, *i.e.*, along the positive x-axis. The principal direction associated with P1 is within 5.83 deg of being normal to the x-axis. Thus, the calculated initial fracture plane should be nearly parallel to the x-axis, which is consistent with the experimental observation (Figure 1).[14]

From the case 2 results (Figures 5 and 6), it is seen that voids less than 50 μm in diameter that are separated from each other by more than 150 μm are unlikely to cause increases in the stress above levels found in isolated voids. P1 stress levels are equivalent to those of case 1. The principal direction associated with P1 is within 1.46 deg of being normal to the x-axis. The calculated initial fracture plane should be almost parallel to the x-axis, as observed experimentally in Figure 1.

The case 3 results (Figures 7 and 8) suggest that fractures should preferentially initiate in deeply embedded voids, rather than in superficial voids, since the

maximum P1 values are lower in surface voids than in deeply embedded voids. In fact, no fractures have been observed to have nucleated at surface voids. The principal direction associated with P1 is within 0.21 deg of being normal to the *x*-axis. Thus, the calculated initial fracture plane should be almost parallel to the *x*-axis, which is consistent with the experimental results (Figure 1, Reference 14).

The case 4 stress distribution (Figure 9), although identical to that of case 1, is nevertheless important. For voids less than 100 μm in diameter in a 4-mm cube, the results strongly suggest that the stress distribution is independent of the diameter. This surprising result is consistent with the case 1 conclusion that the void is located in a semi-infinite medium. It is very similar to the well-known elasticity[19,20] result of a circular hole in an infinite plate under plane stress uniaxial loading. In the elasticity, stress results on the surface of the circular void are independent of the size of the void and maximum principal stress in response to compression loading occurs along the load line. The implication of this conclusion on any effort to improve fatigue performance is that all voids, regardless of size, should be eliminated. It is, thus, insufficient merely to reduce the void size because the stress state cannot be changed.

V. SUMMARY

This study focused on explaining the splitting behavior of Ca BMGs under compression loading. To accomplish this task, finite-element analyses were used to determine the stress states in small spherical voids, and the maximum normal-stress theory of failure was applied. The FEA results were used to accurately predict the crack-nucleation sites and the initial direction of crack propagation, which is generally parallel to the loading direction, as observed experimentally. It was found that adjacent voids do not interact with each other, and cracks should not nucleate from small surface voids. The most important result was that the stress distribution is independent of the void diameter. This trend led to the conclusion that improvements in the fatigue performance should not be expected by reducing the void size.

ACKNOWLEDGMENTS

Two of the authors (GYW and PKL) are very grateful for the support of the National Science Foundation (NSF) International Materials Institutes (IMI) Program (DMR-0231320), Drs. C. Huber, U. Venkateswaran, and D. Finotello, program directors. ONS acknowledges the support of the Air Force Research Laboratory under in-house research Contract No. FA8650-04-D-5233 (UES, Inc.).

REFERENCES

1. A. Inoue: *Acta Mater.*, 2000, vol. 48, pp. 279 306.
2. W.L. Johnson: *MRS Bull.*, 1999, vol. 24, pp. 42 56.
3. H. Choi Yim, R.D. Conner, F. Szuecs, and W.L. Johnson: *Acta Mater.*, 2002, vol. 50, pp. 2737 45.
4. T. Mukai, T.G. Nieh, Y. Kawamura, A. Inoue, and K. Higashi: *Intermetallics*, 2002, vol. 10, pp. 1071 77.
5. W.H. Jiang, G.J. Fan, F.X. Liu, G.Y. Wang, H. Choo, and P.K. Liaw: *J. Mater. Res.*, 2006, vol. 21, pp. 2164 67.
6. H. Li, C. Fan, K. Tao, H. Choo, and P.K. Liaw: *Adv. Mater.*, 2006, vol. 18, pp. 752 54.
7. C. Fan, H. Li, L.J. Kecskes, K. Tao, H. Choo, P.K. Liaw, and C.T. Liu: *Phys. Rev. Lett.*, 2006, vol. 96, p. 145506.
8. B. Yang, C.T. Liu, T.G. Nieh, M.L Morrison, P.K. Liaw, and R.A. Buchanan: *J. Mater. Res.*, 2006, vol. 21, pp. 915 22.
9. O.N. Senkov, D.B. Miracle, and J.M. Scott: *Intermetallics*, 2006, vol. 14, pp. 1055 60.
10. M.L. Morrison, R.A. Buchanan, O.N. Senkov, D.B. Miracle, and P.K. Liaw: *Metall. Mater. Trans. A*, 2006, vol. 37A, pp. 1239 45.
11. O.N. Senkov, D.B. Miracle, V. Keppens, and P.K. Liaw: *Metall. Mater. Trans. A*, 2008, vol. 39A, pp. 1888 1900.
12. K. Amiya and A. Inoue: *Mater. Trans. JIM*, 2002, vol. 43, pp. 81 84.
13. K. Amiya and A. Inoue: *Mater. Trans. JIM*, 2002, vol. 43, pp. 2578 81.
14. G.Y. Wang, P.K. Liaw, O.N. Senkov, D.B. Miracle, and M.L. Morrison: *Adv. Eng. Mater.*, 2009, vol. 11, pp. 27 34.
15. *NEiNastran User's Manual Version 9.2*, Nei Software, Westminster, CA, 2008.
16. Z.Y. Zhang, V. Keppens, O.N. Senkov, and D.B. Miracle: *Mater. Sci. Eng. A*, 2007, vol. 471, pp. 151 54.
17. N.E. Dowling: *Mechanical Behavior of Materials*, 2nd ed., Prentice Hall, Englewood Cliffs, NJ, 1999.
18. A.P. Boresi, O.M. Sidebottom, F.B. Seely, and J.O. Smith: *Advanced Mechanics of Materials*, 3rd ed., John Wiley, New York, NY, 1978.
19. S.P. Timoshenko and J.N. Goodier: *Theory of Elasticity*, 3rd ed., McGraw Hill, New York, NY, 1970.
20. A.E.H. Love: *A Treatise on the Mathematical Theory of Elasticity*, 4th ed., Dover, New York, NY, 1944.